Interannual Variations of the Boreal Summer Intraseasonal Oscillation in the Asian–Pacific Region*

HAIYAN TENG AND BIN WANG

Department of Meteorology, School of Ocean and Earth Science and Technology, University of Hawaii at Manoa, Honolulu, Hawaii

(Manuscript received 9 January 2003, in final form 12 May 2003)

ABSTRACT

A finite-domain wavenumber–frequency analysis was proposed to objectively measure the interannual variability of the boreal summer intraseasonal oscillation (ISO) in the Asian–Pacific region. The strongest interannual variations of the ISO are found in the off-equatorial western North Pacific (WNP). In summers when El Niño is developing, both the westward- and northward-propagating waves with periods of 15–40 and 8–10 days are enhanced in July–October. The northward-propagating ISO in the Indian summer monsoon region, however, has little linkage with El Niño–Southern Oscillation (ENSO).

ENSO affects the northwestward-propagating ISO mode in the WNP through changing the mean circulation. During July–October in the El Niño developing year, the easterly vertical shears over the tropical western Pacific are considerably increased, which in turn promote development and northwestward emanation of Rossby waves away from the equatorial western-central Pacific, reinforcing the WNP ISO. In the Indian summer monsoon region, the ENSO-induced circulation changes are too weak to significantly modify the strong easterly sheared monsoon mean circulation. Therefore, the northward-propagating ISO is insensitive to ENSO.

Unlike the wintertime Madden–Julian oscillation (MJO), which is uncorrelated with ENSO, the May–July MJO is strengthened during El Niño developing years. The questions of why there is a seasonal dependence of the MJO–ENSO relationship and how ENSO directly affects the May–July MJO require further investigations.

1. Introduction

The Madden–Julian oscillation (MJO; Madden and Julian 1971, 1972) arises from equatorially trapped eastward-propagating circulation and convection anomalies. It is the dominant mode of the boreal winter tropical intraseasonal oscillation (ISO). During the boreal summer, the MJO substantially weakens due to northward migration of the warmest sea surface temperature (SST), the intertropical convergence zone and associated maximum boundary layer moist static energy (Wang and Rui 1990; Li and Wang 1994). Meanwhile, the summertime ISO exhibits prominent northward propagation in the Indian monsoon region (Yasunari 1979, 1980; Krishnamurti and Subrahmanyam 1982) and northwestward propagation in the western North Pacific (WNP; Murakami et al. 1984; Lau and Chan 1986). The timescales of the intraseasonal variability in the off-equatorial region are richer than the MJO. For instance, a 10–20-day westward-propagating mode is noted in the off-equatorial Asian summer monsoon region (Krishnamurti and Ardanuy 1980). Higher-frequency variability associated with 6–9 days (Lau and Lau 1990) and 7–21 days (Schrage and Vincent 1996) has also been observed in the WNP. In addition, typhoon activity suggests a 2–3-week periodicity (Frank 1987). All the above features (activity centers, frequency, and propagation) indicate that the canonical MJO cannot sufficiently represent the boreal summer ISO.

The interannual variability of the boreal summer ISO has not been firmly documented, albeit a few authors noticed significant year-to-year irregularities of the northward-propagating ISO in the Indian monsoon region (Yasunari 1980; Vernekar et al. 1993; Mehta and Krishnamurti 1988), and in the WNP (Nitta 1987). Nitta found that the amplitude of the ISO is stronger when local SST is above normal. However, he was unable to detect influence from El Niño–Southern Oscillation (ENSO) from the short record of data. During ENSO cold (warm) events, the enhanced (reduced) 12–24-day westward-propagating monsoon depressions in the Bay of Bengal could be traced upstream to the South China Sea (Chen and Weng 1999).

How ENSO influences the MJO has been controversial, but the general consensus is that the major impact of ENSO is confined in the Pacific. Hendon et al. (1999)

* School of Ocean and Earth Science and Technology Publication Number 6232 and International Pacific Research Center Publication Number 206.

Corresponding author address: Haiyan Teng, Department of Meteorology, University of Hawaii at Manoa, 2525 Correa Road, Honolulu, HI 96822.
E-mail: hteng@hawaii.edu

provided a thorough review. The MJO tends to strengthen in the central Pacific and weaken in the far western Pacific during an ENSO warm event (Gutzler 1991; Fink and Speth 1997). It was speculated that the warm SST in the central Pacific in El Niño facilitates the convective anomalies to propagate farther east, but propagating variances have not been explicitly examined in these studies. Hendon et al. (1999), Slingo et al. (1999), Anyamba and Weare (1995), and Kessler (2001) have tried different measures of the MJO and all found the overall MJO activity is uncorrelated with ENSO. All these studies focused on the boreal winter MJO.

More controversies arise concerning the interannual variations of the boreal summer ISO, partly from lack of an objective and quantitative measurement of the complicated behavior of the summer ISO. The eastward movement of intraseasonal convective anomalies from the equatorial Indian Ocean to the western Pacific is often accompanied by northward propagation toward the Indian subcontinent (e.g., Anamalai and Slingo 2001). There are other occasions that the northward-propagating intraseasonal convections in the Indian Ocean are independent from the equatorial eastward-propagating convections (Wang and Rui 1990), especially after late July when the western Pacific monsoon breaks out and the equatorial eastward propagation substantially weakens (Kemball-Cook and Wang 2001). Such complexity requires careful and objective measures of the boreal summer ISO. In this paper, we extend the wavenumber-frequency spectral analysis from a global domain to a regional domain to quantify the strength of the eastward, northward, and westward propagations.

The present analysis documents the interannual variations of the boreal summer ISO, which covers the entire Asian–Pacific summer monsoon region (section 3). The mechanisms for the interannual variability are discussed in terms of the equatorial wave dynamics and response of the monsoon to ENSO forcing (section 4). The main results are summarized in section 5.

2. Data and analysis method

a. Data

The primary datasets include 1979–2001 daily outgoing longwave radiation (OLR; Liebmann and Smith 1996) from operational polar-orbiting satellites, 1979–2001 pentad-mean Climate Prediction Center (CPC) Merged Analysis of Precipitation (CMAP; Xie and Arkin 1997) and 1958–2001 daily National Centers for Environmental Prediction–National Center for Atmospheric Research (NCEP–NCAR) reanalysis (Kalnay et al. 1996). All datasets have a $2.5^\circ \times 2.5^\circ$ global coverage. OLR is employed to depict convection in wavenumber–frequency analysis because it has a daily temporal resolution while the finest resolution of the CMAP is pentad mean. Zonal and meridional propagations are quantitatively cross-examined using both OLR and circulation variables from the NCEP–NCAR reanalysis. Since the quality of the reanalysis dataset has been dramatically improved in the mid-1970s after satellite observation became available, we cautiously avoid drawing the conclusions upon the early decade's data.

The 1958–2001 CPC Niño-3.4 (5°S–5°N, 170°–120°W) SST anomalies are used to categorize ENSO events. Our study focuses on the boreal summer season from May to October, hence we select El Niño (La Niña) summer by May–October mean Niño-3.4 anomaly above (below) one standard deviation (about 0.7°C). Following such a criterion, 1963, 1965, 1972, 1982, 1987, 1991, and 1997 are identified El Niño summers, while 1964, 1970, 1973, 1975, 1988, 1998, and 1999 are La Niña summers.

The intraseasonal component y_{iso} is defined as the sum of Fourier components with period longer than 10 days and shorter than 90 days. In order to extract y_{iso} the sum of the annual mean and the first four harmonics (y_{ac}) are removed from each year's time series. The interannual variation of the seasonal mean, which is carried by y_{ac}, is removed. Upon performing such filtering at each grid point, standard deviations are used to represent the amplitude of ISO. To further separate stationary anomalies from propagating anomalies, wavenumber-frequency analysis is performed.

b. Finite domain wavenumber–frequency analysis

Unlike variations such as ENSO or tropical cyclones, the ISO is more difficult to measure. Quantification of the boreal summer ISO is even more challenging due to its complicated propagation characteristics. Conventional methods, such as the Hovmöller diagram, the extended EOF, or the complex EOF analysis have difficulties in quantitatively measuring wave propagation, especially dispersive waves. The intensity, propagation, and frequency, which are intrinsic wave properties, are usually studied separately.

Closely resembling the normal mode method in theoretical studies, the wavenumber–frequency analysis transforms a time series from a spatial–time domain to a wavenumber–frequency domain (Hayashi 1982). Thus, variability associated with different frequencies, spatial scales, and propagation directions are separated. Salby and Hendon (1994) applied wavenumber–frequency decomposition to filter the MJO signal. Hendon et al. (1999) further constructed a MJO index using the filtered MJO signals and studied its interannual variations. Their index showed generally consistent interannual variations of the MJO as revealed by Slingo et al. (1999). Using a similar wavenumber–frequency analysis method, Wheeler and Kiladis (1999) identified the dispersion relationship of the tropical waves, verifying in part the theory of Matsuno (1966). These wavenumber–frequency analyses do not distinguish the propagating variances from stationary variances. Inside the category of wavenumber–frequency analysis, detailed

methodology for calculating the spectrum of propagating waves varies from study to study (reviewed by von Storch and Zeiers 1999). Hayashi's (1982) formalism is adopted in the present work. Variances of the anomalies propagating in opposite directions are estimated by the cospectrum between two Fourier spatial decomposition coefficients, namely, the coefficients for sine and cosine functions. Conventionally, the spatial decomposition is carried out along a full latitudinal circle as is granted by the earth's spherical boundary condition. The wavenumbers are discrete integers from 0 to $n_{\text{lon}}/2$, where n_{lon} is the total number of the grid points at given latitude.

We extend the wavenumber–frequency analysis from a global domain to a finite domain. This is because the boreal summer ISO is effectively trapped in the northern summer monsoon region by the lower boundary conditions (such as SST, land, and ocean surface moisture distribution), and the mean three-dimensional monsoon flows (Wang and Xie 1997). The assumption underlying the regional wavenumber–frequency spectral analysis lies in the fact that these summer ISO modes nearly vanish at the two ends of certain latitude or longitude domains. Numerous computations have been performed to assure the insensitivity of the results to the choice of the longitude (latitude) domains. Finite domain wavenumber–frequency analysis reveals detailed regional characteristics, which are overwhelmed in the global domain analysis.

For the summertime MJO, we mainly focus on the wavenumber-1 anomalies from 40°E to 180° in May–July, although its averaged behaviors in May–October and August–October have also been investigated. For the off-equatorial westward-propagating ISO, we zoom to 100°E–180° in the western North Pacific in July–October, where this mode has been observed. Choice of the two different temporal and spatial domains is based on the subseasonal change in the ISO's characteristics according to case studies (Kemball-Cook and Wang 2001) and Hovmöller diagrams at different latitudes.

The northward-propagating ISO in the Asian–Pacific summer monsoon region is normally restricted to the latitudinal domain from 0° to 25°N. The equatorial region and the off-equatorial region often posses opposite active (break) phase, which compromises the ascending (descending) branch of a transient meridional circulation. Such a meridional dipole pattern is primarily described by the meridionally propagating wavenumber-1 mode in the wavenumber–frequency analysis. Therefore, we chose a spatial decomposition domain of 5°S–25°N, and examined the wavenumber-1 component.

c. Significance test

Two-sample Student's *t* tests are applied to test the significance of composite scenarios for ENSO warm and cold episodes. The null hypothesis for the two-sample Student's *t* test is that warm and cold ensembles have identical sample means. Test statistics are constructed following the convection (refer to Wilks 1995, chapter 5). Student's *t* test is also used for testing the significance of correlation coefficients.

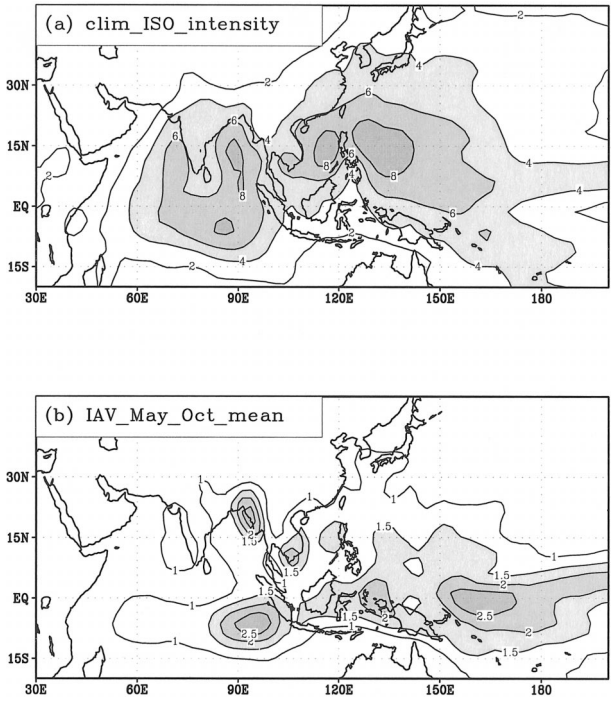

FIG. 1. (a) 1979–2001 averaged boreal summer ISO intensity and (b) the 23-yr std dev of May–Oct seasonal mean in CMAP. Both units are mm day^{-1}.

3. Interannual variations of the boreal summer ISO

a. Overall intensity

The overall intensity of the summertime ISO is measured by the standard deviation of May–October intraseasonal anomalies. This intensity varies from year to year. Figure 1a displays the 23-yr (1979–2001) mean ISO intensity in CMAP. The largest amplitude of the ISO is located along 15°N over the Philippine Sea, the South China Sea, the Bay of Bengal, and the eastern Arabian Sea. Other active center is found in the south Indian Ocean at about 5°–10°S. The results derived from the 850-hPa wind are consistent in the tropical region (figure not shown). Besides the 850-hPa wind also shows large intraseasonal variability at higher latitudes.

The variability center of the summertime ISO is located away from the equatorial region where the most pronounced year-to-year variation in the summer mean state is found. Figure 1b shows the standard deviation of the May–October mean CMAP that represents the interannual variation of the summer mean state. The most significant interannual variation of seasonal mean state is located at the equatorial western central Pacific,

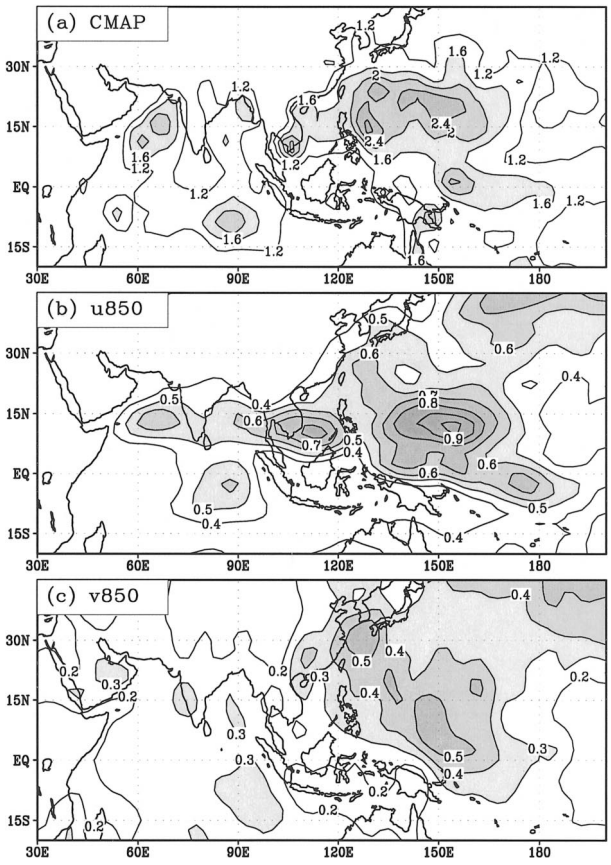

FIG. 2. 1979–2001 interannual std devs of the boreal summer ISO intensities using (a) CMAP, (b) 850-hPa zonal wind, and (c) 850-hPa meridional wind. The units are mm day^{-1}, m s^{-1}, and m s^{-1} for (a), (b), and (c), respectively.

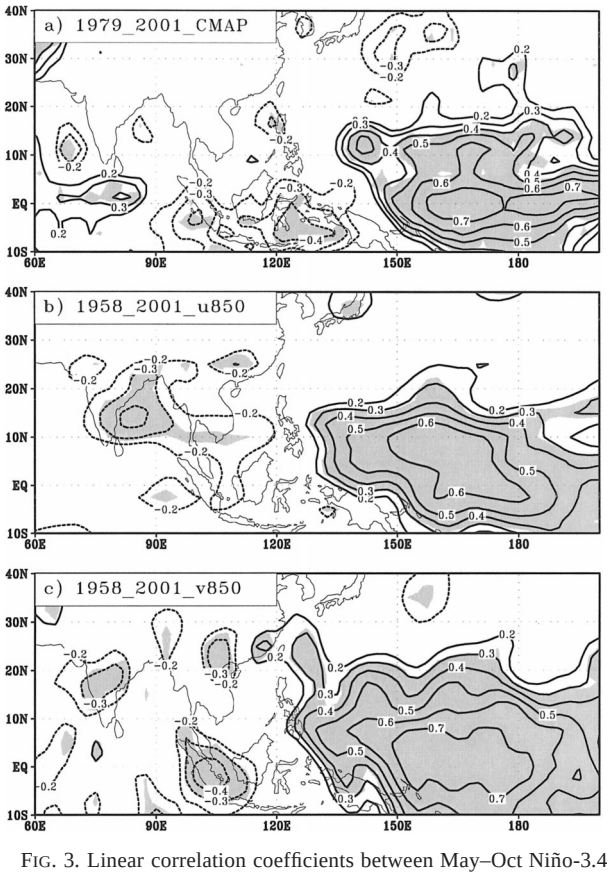

FIG. 3. Linear correlation coefficients between May–Oct Niño-3.4 SST anomaly and the summer ISO intensities in (a) CMAP during 1979–2001, (b) 850-hPa zonal, and (c) 850-hPa meridional winds during 1958–2001. Shading indicates the 95% confidence level. Contours with values between −0.2 and 0.2 are omitted.

which is induced by ENSO. The second maximum is located at 5°S, west of Sumatra. It is noted that the variation of the ISO favors the off-equatorial region while the interannual variations of the summer mean state favor the equatorial region.

The most pronounced interannual variation of the summertime ISO intensity is located in the western North Pacific. Figure 2 shows the interannual standard deviations of the 23-yr ISO intensity in CMAP and 44-yr ISO intensities in 850-hPa zonal and meridional winds (also refer to as u_{850}, v_{850}). Although climatologically the Bay of Bengal is the most active center for the summertime ISO, its interannual variation is substantially weaker than in the WNP. The longitude domains of the year-to-year variability centers are similar in the three variables, but the latitudes slightly differ. The CMAP centers along 15°–20°N while the elongated band of u_{850} variability is centered at about 10°N. This latitudinal phase shift between convection and zonal wind is consistent with the positive correlation between an enhanced convection and associated enhanced westerly to the south and southwest of the convection shown by Wang and Fan (1999), who interpret this relation as resulting from the interaction between convective heating and Rossby wave response. The v_{850} ISO interannual variability center exhibits a northwestward tilt from about 160°E at the equator to the East China Sea. It indicates that the meridional wind anomalies associated with anomalous cyclone/anticyclone prevail along this tilted path.

The interannual variation in the ISO intensity is linked to ENSO. Linear correlation coefficients between the ISO intensity at each grid and the May–October seasonal mean Niño-3.4 SST anomalies are presented in Fig. 3. To detect decadal variability embedded in the 44-yr ISO intensities in u_{850} and v_{850}, correlations in the following two periods are calculated: 1958–2001 (Figs. 3b,c) and 1979–2001 (figure not shown). For both cases, positive correlations dominate in the WNP. The positive area tilts from southeast toward northwest. The axis of the maximum positive correlation coincides with the NWP monsoon trough. Significant negative correlations are seen in the western Bay of Bengal between 10° and 20°N. The negative correlations, however, become insignificant for the latter 1979–2001 period. Significant positive correlations are also found in the WNP in

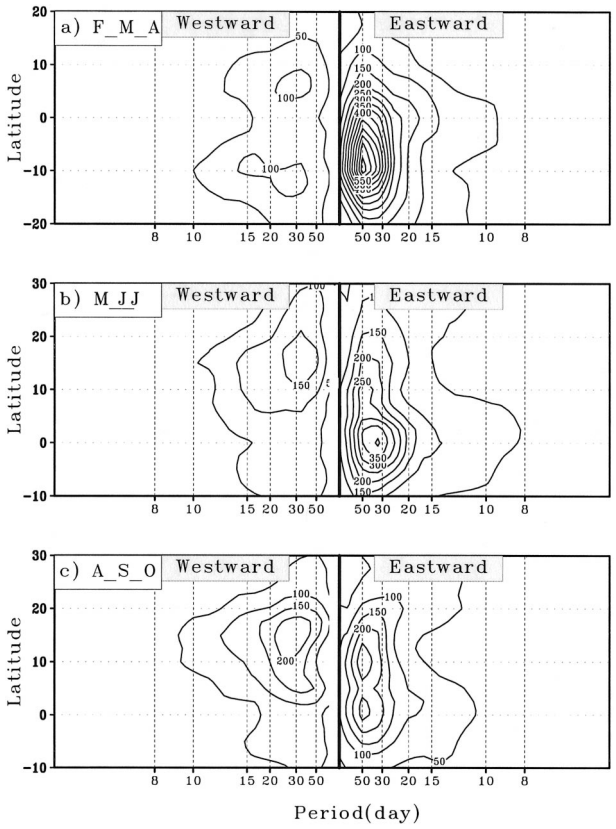

FIG. 4. 1979–2001 mean spectra as a function of latitude and period for zonally propagating wavenumber-1 OLR anomalies at 40°E–180° in (a) Feb–April, (b) May–Jul, and (c) Aug–Oct. Wavenumber 1 corresponds to a wavelength of 140° lon.

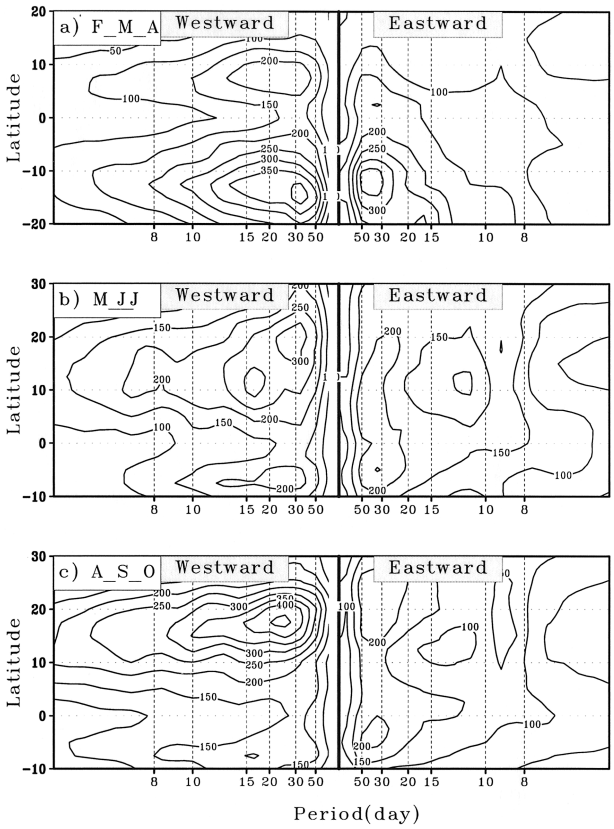

FIG. 5. 1979–2001 mean spectra as a function of latitude and period for zonally propagating wavenumber-2–10 OLR anomalies at 40°E–180° in (a) Feb–April, (b) May–Jul, and (c) Aug–Oct.

CMAP rainfall data, with the maximums between 0° and 10°N (Fig. 3a). There is a small positive-correlation area in the equatorial central Indian Ocean and a negative-correlation area in the eastern Arabian Sea at 10°N. The correlation coefficients in the rest of the Indian monsoon region are insignificant. The ISO intensity shows the most significant correlation with Niño-3.4 SST in the western and central Pacific.

Thus, both convection and lower-tropospheric circulation show pronounced interannual variation in the ISO intensity in the WNP, which is closely linked with ENSO. But whether and how ENSO affects the ISO in the Indian monsoon region remain to be explored.

b. The MJO

The convective anomalies of the wintertime MJO can travel farther east of 150°W, but are restricted to the Eastern Hemisphere in the boreal summer. Therefore we choose 40°E–180° as the spatial decomposition domain for the summertime MJO. Figure 4 shows the strength of the zonal propagation by spectrum density of the wavenumber-1 (wavelength of 140° of longitude) OLR anomalies spanning between 40°E and 180°. Due to change in the ISO behavior within the summer (Kemball-Cook and Wang 2001), we calculated the spectra in May–July and July–October separately. In order to show that the MJO dramatically weakens in the summer, the spectrum is also calculated for the period of February–April. We chose the same 3-month temporal length and the same spatial domain to facilitate comparison.

The 23-yr averaged spectrum in February–April is dominated by a 50-day eastward propagation (Fig. 4a), which reflects the main characteristics of the MJO. It is most pronounced between 0° and 15°S. Meanwhile, weak westward-propagating anomalies are found at 5°–10°N and 10°S. Although the westward-propagating anomalies outweigh the eastward-propagating ones at higher wavenumbers (Fig. 5a), the total variance of wavenumbers 1–10 is dominated by the eastward propagation in the winter.

In May–July (Fig. 4b), the MJO center moves to the equator. The variance decreases to about half of that in February–April. The dominant period is 30–50 days with the peak closer to 30 days. The westward-propagating ISO center in the Southern Hemisphere vanishes in the wavenumber-1 anomalies but remains evident in higher wavenumbers at 5°S (Fig. 5b). The westward-

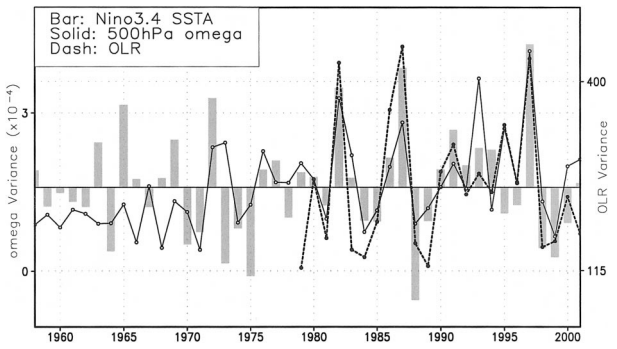

FIG. 6. May–Jul MJO index in 500-hPa vertical velocity (solid) during 1958–2001, the OLR MJO index (dash) during 1979–2001, and May–Jul mean Niño-3.4 SST anomaly (bar) during 1958–2001. The MJO index is defined as the mean spectrum density for 20–50-day eastward-propagating wavenumber-1 (at 40°E–180°) anomalies averaged at 2.5°S–5°N for the vertical velocity and at 5°S–10°N for OLR.

propagation center in the Northern Hemisphere is located between 10° and 20°N. The total variance of wavenumbers 1–10 indicates a prevailing eastward propagation at the equator and significant westward propagation along 15°–20°N.

In August–October (Fig. 4c), the MJO continues to weaken at the equator. There are two bands of eastward-propagating anomalies at 0° and 10°N. The oscillating period is prolonged to 50 days, similar as in the winter. The variance of the westward-propagating ISO has grown in both wavenumber 1 (Fig. 4c) and wavenumbers 2–10 (Fig. 5c). The variance of wavenumbers 1–10 is dominated by westward propagation between 10° and 20°N. Switch of the dominance from the MJO in May–July to the off-equatorial westward-propagating ISO in August–October is associated with the monsoon annual cycle. The major rainfall in early summer is located at the Indian monsoon region, but in late summer is found over the WNP (LinHo and Wang 2002).

In order to measure the intensity of the MJO in May–July, wavenumber–frequency analyses were carried out for the longitudinal domain of 40°E–180° in the equatorial zonal plane using 1958–2001 500-hPa vertical velocity (hereafter referred to as ω_{500}) and 1979–2001 OLR. The MJO index is defined as the averaged spectrum density of 20–50-day wavenumber-1 anomalies at 2.5°S–5°N, 40°E–180° for ω_{500} and 5°S–10°N for the OLR. These domains are the variability centers of the eastward-propagating intraseasonal OLR (Fig. 4b) and ω_{500} (figure not shown) anomalies.

Both the OLR and the ω_{500} indices have a close connection with Niño-3.4 SST anomalies (Fig. 6). The correlation coefficients between the MJO indices (using OLR and ω_{500}) and Niño-3.4 SST for the period of 1979–2001 are listed in Table 1. It suggests that the MJO is enhanced in May–July during the initial developing stage of El Niño. The correlation remains significant when we enlarge the domain to 10°S–10°N, 40°–220°E for OLR. Based on the OLR index, we have compared Hovmöller diagrams of the strong MJO summers with the weak ones and found that the strong summers not only have more pronounced intraseasonal anomalies over both oceans, their eastward propagations are also better organized (figure not shown).

TABLE 1. Correlation coefficients between the May–Jul MJO indices using 500-hPa vertical velocity (ω_{500}), OLR, and the Niño-3.4 SST anomaly during 1979–2001. All three correlation coefficients are significant at the 95% confidence level.

	ω_{500} MJO index	OLR MJO index	Niño-3.4 SST
ω_{500} MJO index		0.73	0.77
OLR MJO index			0.72

The enhanced May–July MJO is not correlated with the local SST in the Indian Ocean. Correlation coefficients were calculated between the OLR MJO index and May–July mean SST from the NCEP–NCAR reanalysis during 1979–2001 (figure not shown). There are small areas of positive correlations in the north Arabian Sea and at 15°S east of Madagascar. No significant correlation is found in the equatorial Indian Ocean. Meanwhile, negative (positive) correlation dominates the Maritime Continent (the Pacific east of 160°E). These patterns are similar to the distribution of the ENSO-induced SST anomaly. The correlation further confirms that ENSO affects the May–July MJO. The Indian Ocean SST, however, does not directly influence the strength of the MJO.

The tight MJO–ENSO correlation in May–July is in a sharp contrast with the insignificant correlation previously found between the boreal winter MJO and ENSO. To confirm the previous results, a wintertime MJO index is constructed following a similar procedure, except that the spatial–temporal domain is switched to 30°E–110°W in November–April. Variances of the wavenumber-1 (wavelength of 220° of longitude) eastward-propagating OLR anomalies are averaged between 15°S and 5°N. We also employed the MJO index proposed by Slingo et al. (1999). Variance of the 20–100-day-filtered 200-hPa global mean zonal wind is calculated in November–April during 1979–2001 to represent the MJO intensity in each winter. Our wintertime MJO index is highly correlated with the Slingo et al. (1999) index. The correlation coefficient is 0.77 ($n = 22$ winters), significant at the 95% confidence level. Both indices show poor connection with ENSO.

c. *Westward-propagating ISO in the western North Pacific*

The WNP ISO has a predominant northwestward propagation (Lau and Chan 1986). For convenience, we examine the ISO in longitudinal and meridional directions separately. Here we first focus on the westward-propagating component. The northward-propagating

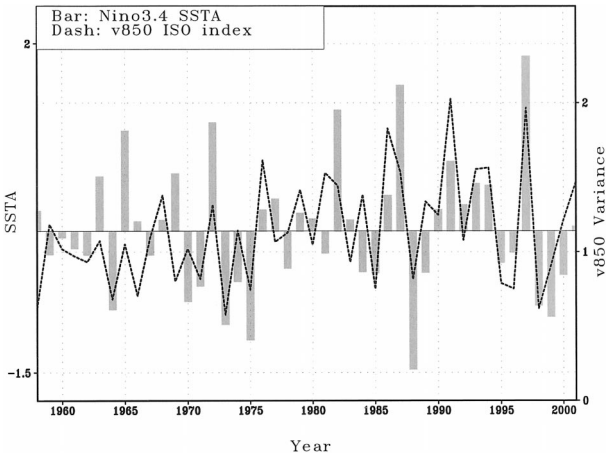

FIG. 7. 1958–2001 Jul–Oct mean Niño-3.4 SST anomaly (bar) and mean spectrum density of 10–50-day wavenumber-1–3 (at 100°E–180°) westward-propagating 850-hPa meridional wind anomaly (dash) at 5°–20°N. Wavenumber 1 corresponds to a wavelength of 80° lon.

component will be examined in the next section. Because the westward propagation is more pronounced from July to October and is confined to the longitude domain between 100°E–180°, we select them as the spatial and temporal domain for wavenumber–frequency analysis.

The ISO intensity in v_{850} has the most pronounced correlation with ENSO, thus we use it to define the westward-propagating ISO index. A total of seven wavenumber–frequency spectrum diagrams are produced for each 2.5° latitude bin between 5° and 20°N in 1958–2001. The westward-propagation index was constructed by averaging the spectrum density associated with wavenumbers 1–3 and 10–50-day westward-propagating v_{850} anomalies between 5° and 20°N. We did not expand the latitude domain farther north, because the large variability center in the East China Sea may be associated with the midlatitude intraseasonal oscillation (Fig. 2c).

The westward-propagation index (Fig. 7) has significant (at the 95% confidence level) positive correlation with Niño-3.4 SST, with the 44-yr correlation coefficient of 0.62. The index also suggests an interdecadal change in the mid- or late-1970s with the earlier epoch (1958–78) having weaker westward-propagating ISO. We are uncertain whether the interdecadal change is caused by inhomogeneity of the data.

The westward-propagating ISO exhibit multiscales, therefore it is important to examine more wavenumbers. Because wavenumbers 1–3 possess most of the variance, their spectrum densities at different latitudes are correlated with the Niño-3.4 SST. Figure 8 shows the correlation coefficients with the Niño-3.4 SST for wavenumber-1, -2, and -3 v_{850} anomalies between 100°E–180°, respectively. Significant correlations are found between ENSO and the wavenumber-1 and -2 westward-

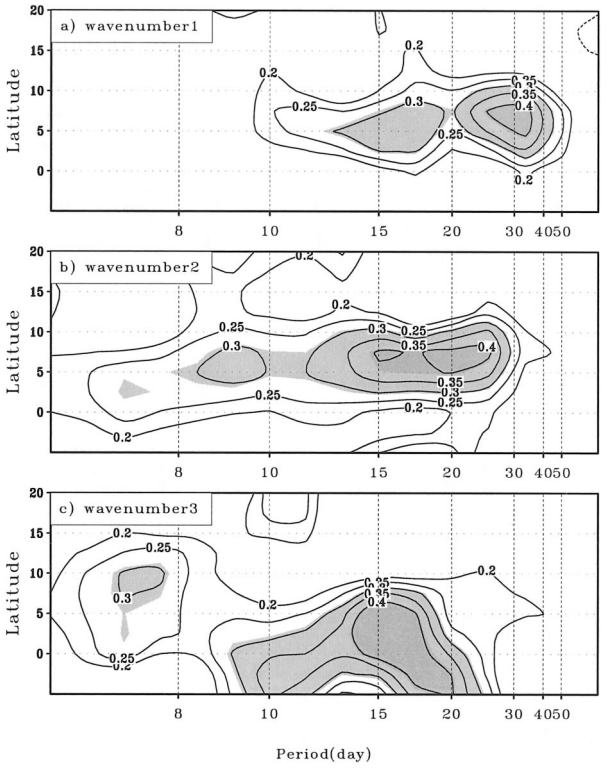

FIG. 8. Correlation coefficients between the 1958–2001 Niño-3.4 SST anomaly and spectrum density of the westward-propagating intraseasonal anomalies of v_{850} as a function of latitude and period. (a)–(c) Wavenumber-1, wavenumber-2, and wavenumber-3 westward-propagating anomalies within 100°E–180°, respectively. Shading indicates the 95% confidence level. Contours with values between −0.2 and 0.2 are omitted.

propagating v_{850} anomalies between 5° and 10°N and the wavenumber-3 anomalies between 5°S and 10°N. For wavenumber-1, -2, and -3 v_{850} anomalies, the significant periods are about 30, 20, and 15 days. Besides, higher frequencies (period ~8 days) are also significantly correlated with ENSO warming at about 10°N.

d. Northward-propagating ISO

In order to examine the poleward-propagating ISO, wavenumber–frequency analyses are carried out at the meridional direction. There are total of 70 spectra for each 2.5° longitudinal stripe between 40°E and 167.5°W. By choosing the spatial decomposition domain from 5°S to 25°N, the analysis yields variance density of the northward-propagating intraseasonal anomalies. Only the wavenumber-1 anomaly at this domain is considered, because it possesses dominant variance. We also tested the sensitivity of the results to choices of the domain (e.g., 0°–20°N). The main results are insensitive to the changes.

Figure 9a shows the 44-yr-averaged spectrum for u_{850}. Three longitude bands of strong northward-propagating ISO are identified at 70°–90°, 110°–120°, and 125°–

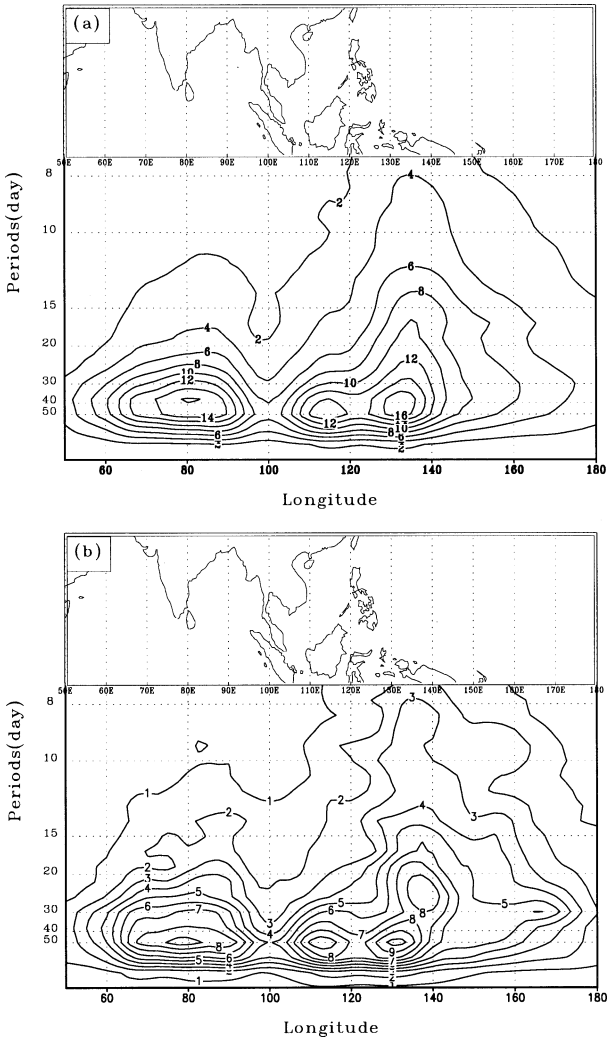

FIG. 9. (a) Mean and (b) std dev of 1958–2001 spectra as a function of longitude and period for wavenumber-1 northward-propagating 850-hPa zonal wind anomalies in May–Oct. The reference map shows the meridional spatial decomposition domain (5°S–25°N) and longitudinal domain of interest.

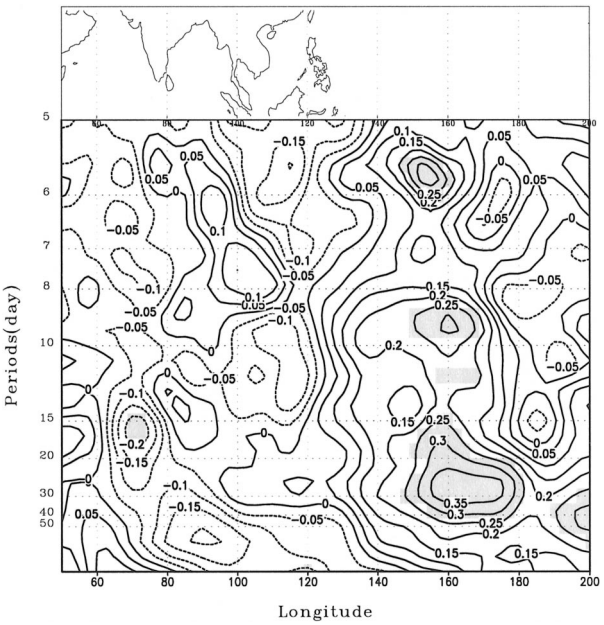

FIG. 10. Linear correlation coefficients of the spectrum density for the wavenumber-1 northward-propagating u_{850} anomalies with reference to the Niño-3.4 SST anomaly in the period of 1958–2001. Shading indicates the 95% confidence level. Nine-point smoothing has been applied on the coefficients.

140°E. The dominant period is about 30–50 days over the Indian Ocean and the Indian peninsula. The spectrum broadens over the Philippine Sea. Higher-frequency wave activities with oscillating period below 20 days are enhanced. The 23-yr-averaged spectrum for OLR (figure not shown) shows similar features, except that it has a separate northward propagation center at 65°–75°E in the Arabian Sea with a dominant period of 30–50 days. Unlike in the u_{850} spectrum where all three northward propagation centers have similar strength, the OLR spectrum reveals that the Bay of Bengal has the largest variance associated with the 30–50-day northward-propagating anomalies. The maximum contours in the averaged OLR spectrum at the Bay of Bengal, the Arabian Sea, the Philippine Sea, and the South China Sea are 700, 600, 500, and 400 $(\mathrm{W\ m^{-2}})^2$, respectively.

The year-to-year variability of the northward-propagating ISO is measured by interannual standard deviation of the 44-yr u_{850} spectrum (Fig. 9b) and of the 23-yr OLR spectrum (figure not shown). Considering the 30–50-day anomalies, the locations with large interannual variations roughly coincide with the climatological active centers. The notable feature is the pronounced interannual variations of the 20–30-day mode over the Philippine Sea. Besides, there is a small tongue sticking out from a 40-day period in the Philippine Sea to a 30-day period at the date line, indicating a relatively large interannual variation. The standard deviation in the OLR spectrum (figure not shown) suggests that although the 30–50-day northward-propagating ISO is weaker in the Philippine Sea than in the Indian Ocean, its interannual variability is more pronounced compared with those in the Indian Ocean. In addition, the 15–20-day oscillation over the Arabian Sea and the Bay of Bengal also shows relatively large interannual variation in the OLR spectrum.

To find the relationship between ENSO and the northward-propagating ISO, we calculated the linear correlation coefficients between the spectrum density and the Niño-3.4 SST (Figs. 10 and 11). Significant positive correlations with the u_{850} spectrum are found from 150°E to the date line at 15–50, 9, and 6 days (Fig. 10). The positive correlations drop sharply and become insignificant when crossing the South China Sea. Slightly significant negative correlations are found in the Arabian Sea at 70°–80°E at an oscillating period of 15–20 days. The negative correlations in the Arabian Sea are much

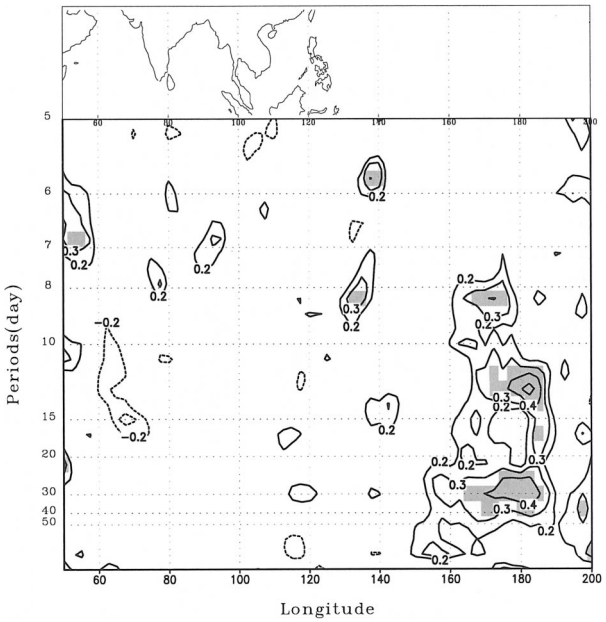

FIG. 11. Same as Fig. 10 but for correlation with the OLR spectrum during 1979–2001. Contours with values between −0.2 and 0.2 are omitted.

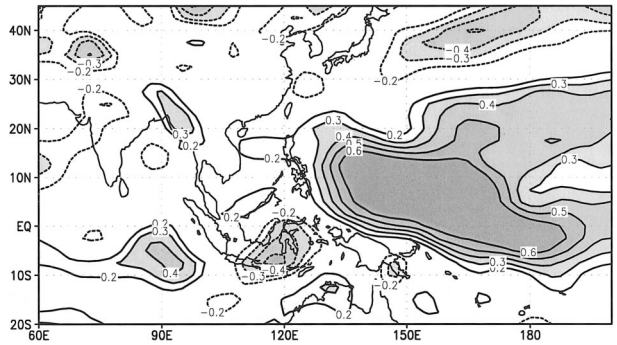

FIG. 12. Correlation coefficients between the boreal summer ISO intensity and May–Oct seasonal mean state both using 850-hPa zonal wind in the period of 1958–2001. Shading indicates the 95% confidence level. Contours with values between −0.2 and 0.2 are omitted.

weaker than the positive correlations in the Pacific regarding to both the absolute values of the correlation coefficient and the spatial areas that possess a statistical significance. Correlation coefficients between the 23-yr OLR spectrum and the Niño-3.4 SST are less significant (Fig. 11). Positive correlation is restricted to 160°E–170°W with enhanced 30-day, biweekly, and 8–10-day oscillations in El Niño.

As a summary, the boreal summer ISO exhibits larger year-to-year amplitude change over the WNP than in the Indian monsoon region. The wavenumber–frequency spectrum suggests that the westward and northward propagations of the ISO in the WNP are significantly associated with ENSO condition. When the central-eastern Pacific warms up in the boreal summer, the ISO is enhanced in the WNP with stronger westward- and northward-propagation components with periods of 15–40 and 8–10 days. El Niño can also significantly enhance the May–July MJO. The northward-propagating ISO in the Indian monsoon region does not seem to be sensitive to ENSO.

4. Why is the western North Pacific ISO intimately linked to ENSO?

The WNP has the largest interannual variation in the strength of the summertime ISO (Fig. 2). It is unclear how ENSO can influence the ISO in the off-equatorial western Pacific and Southeast Asia, given the fact that the seasonal mean circulation is primarily affected by ENSO in the equatorial western Pacific (Fig. 1b).

Figure 12 shows linear correlation coefficients between the 44-yr boreal summer ISO intensity and the May–October seasonal mean, both using 850-hPa zonal wind. Significant positive correlation prevails in the WNP from 0° to 20°N, whereas significant negative correlations are over the central Maritime Continent. In the Indian monsoon region, significant correlation is only found over the upper Ganges River valley. Compared with the ISO in the Indian monsoon region, the ISO in the WNP is found more sensitive to change in summer's mean state.

Theoretical studies have demonstrated that the vertical shear of zonal flows has a remarkable impact on Rossby wave and westward-propagating mixed Rossby–gravity waves (Wang and Xie 1996; Xie and Wang 1996). Easterly vertical shears (easterly wind increases with height) can enhance Rossby wave in the lower troposphere, whereas westerly shear tends to trap Rossby waves in the upper troposphere. Furthermore, in the presence of moist convection, enhanced low-level perturbation increases boundary layer moisture convergence, which in turn interacts with convective heating. Therefore, enhanced easterly shear favors amplification of moist equatorial Rossby waves.

Climatologically, the western Pacific is a transition area between easterly and westerly shears (Fig. 13a). Yet the western Pacific region has the most pronounced interannual variation associated with ENSO (Fig. 13b). Because the western Pacific has a weak vertical shear, it is easier for ENSO-induced circulation anomalies to reverse the sign of the vertical wind shear and cast dramatic impacts on Rossby wave response. When there is a basinwide warming in the central-eastern Pacific, it induces westerly anomalies in the lower troposphere and easterly anomalies in the upper troposphere over the western Pacific, which results in pronounced vertical shear changes between El Niño and La Niña summers (Fig. 13b). The change in vertical shear (about half of the difference of Fig. 13b) in El Niño and La Niña summers is comparable to the climatological mean shear in the WNP. In western India and the equatorial eastern Indian Ocean, there is a weak decrease/increase of east-

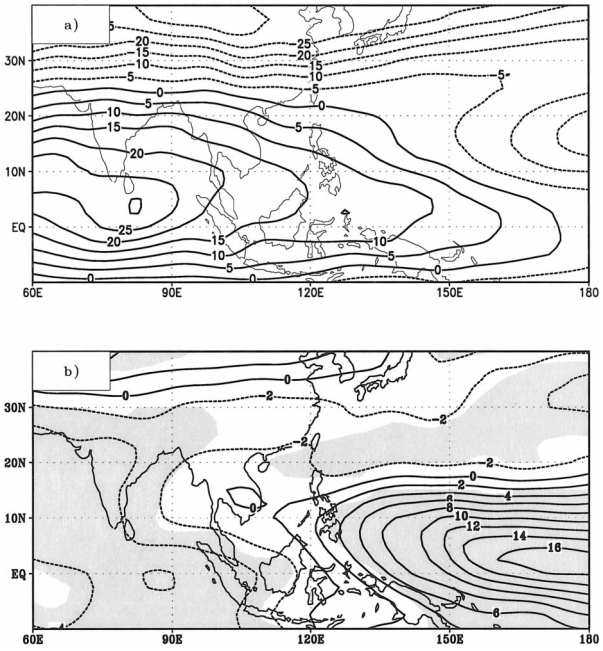

FIG. 13. (a) 1958–2001 May–Oct averaged $u_{850} - u_{200}$ shear; (b) May–Oct $u_{850} - u_{200}$ shear difference between seven strong El Niño summers (1963, 1965, 1972, 1982, 1987, 1991, 1997) and seven strong La Niña summers (1964, 1970, 1973, 1975, 1988, 1998, 1999). Shading indicates the two-sample t test's 95% confidence level.

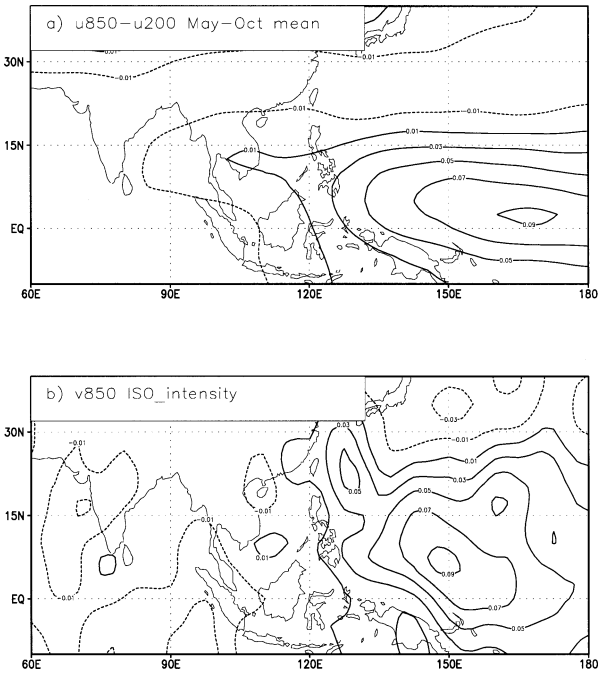

FIG. 14. The dominant SVD mode between (a) May–Oct mean $u_{850} - u_{200}$ vertical wind shear and (b) the v_{850} boreal summer ISO intensity in Jul–Oct 1979–2001. They account for 84.6% of the total covariance, compared with 5.6% from the second dominant mode. The dominant mode of the vertical shear in (a) contributes to 49.4% of its total variance. The dominant modes of the boreal summer ISO intensity in (b) contribute to 26.5% of its total variance. Correlation between the two temporal coefficients of the first SVD mode is 0.94.

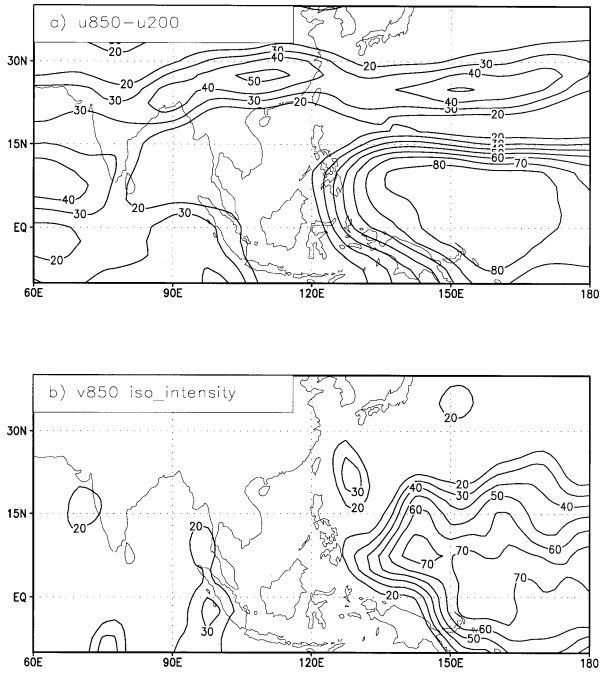

FIG. 15. Fractional variance that the first SVD mode (Fig. 14) contributes to the interannual variances of (a) the mean $u_{850} - u_{200}$ and (b) the boreal summer ISO intensity using v_{850} at each individual grid point in Jul–Oct from 1979 to 2001. The values are given in percentages. Contours with values less than 20 are omitted.

erly shear in the El Niño/La Niña summers. But they are only a moderate fraction of the mean shears.

The dominant interannual modes of the summer ISO intensity in v_{850} (Fig. 14b) are related to summer mean vertical shear (Fig. 14a). The dominant singular vector decomposition (SVD) mode between the mean vertical wind shear and v_{850} ISO intensity accounts for 84.6% of their total covariance, far ahead of the second mode (5.6%). The correlation coefficient between the temporal coefficients is 0.94. In the first mode, the pattern of the mean vertical shear resembles the ENSO anomaly pattern in Fig. 13. It contributes 49.4% of its total variance. The SVD pattern for the ISO intensity mirrors that of the interannual ISO variability in the WNP (Fig. 2c). It explains 26.5% of the total variance. Both patterns resemble their individual dominant empirical orthogonal function (EOF; figure not shown). From the first SVD mode, the reconstructed mean vertical shear and the v_{850} ISO intensity both contribute more than 50% of its individual interannual variance in the WNP (Fig. 15).

The weak mean monsoon vertical wind shear and its strong interannual variation cause the ISO to have larger interannual variations in the WNP than in the Indian monsoon region. During El Niño, the enhanced mean easterly vertical shear over the WNP is responsible for the enhanced emanation of the moist equatorial Rossby waves. These waves have a periodicity of 8–10 days but their amplitude is modulated in 30–40-day timescale due to vigorous air–sea interaction (Kemball-Cook and

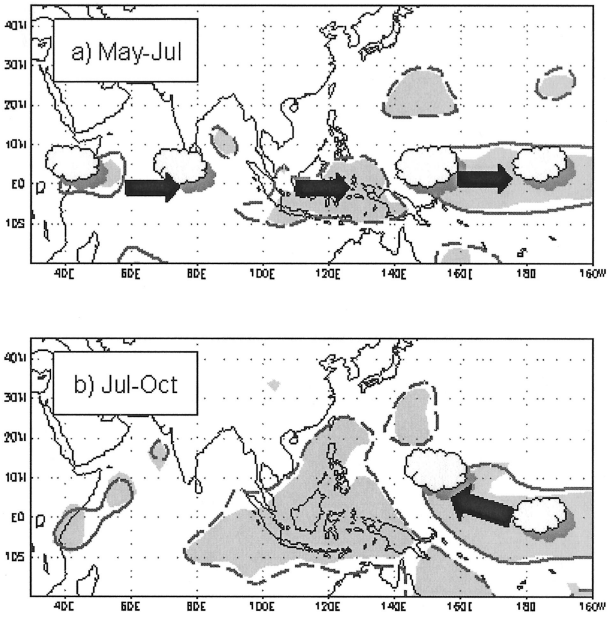

FIG. 16. Schematic diagram that describes how El Niño modifies (a) the May–Jul MJO and (b) the northwestward-propagating ISO in Jul–Oct. Solid and dash contours indicate the region where (a) May–Jul and (b) Jul–Oct mean CMAP rainfall has positive and negative correlations with May–Oct mean Niño-3.4 SST. Shading within the contour shows correlation above the 95% confidence level. Black arrow denotes that the MJO is enhanced in May–Jul in (a) and that the northwestward-propagating ISO is enhanced over the western North Pacific in Jul–Oct in an El Niño summer in (b).

Wang 2001). This leads to an enhanced ISO on timescales of 30–40 and 8–10 days.

5. Concluding remarks

The main goal of this study is to document the year-to-year variability of the boreal summer ISO, including the MJO in May–July, the northwestward-propagating mode in the WNP in July–October and the northward-propagating mode in the entire summer monsoon domain. Indices based on the wavenumber–frequency spectrum are defined for each of the ISO modes to quantify their interannual variability.

Unlike the wintertime MJO, the May–July MJO and the July–October northwestward-propagating ISO mode in the WNP are sensitive to ENSO. How El Niño modifies these modes is summarized in Fig. 16. During May–July, the Niño-3.4 SST anomaly is usually mild compared with its peak phase in the winter, but it causes significant remote impacts in the Indo-Pacific monsoon region. Enhanced mean rainfall at the East African coast and the western Indian Ocean and suppressed rainfall in the Maritime Continent are produced. There is also deficient rainfall at 10°N in the Bay of Bengal. The overall MJO is enhanced, despite the fact that local intraseasonal variability in the Maritime Continent does not intensify. The arrows in Fig. 16a denote enhanced eastward propagation. After the WNP monsoon breaks out in July, enhanced convection band protrudes to 10°N in the WNP and suppressed mean rainfall area expands to Taiwan and the ocean to the southeast of Japan (Fig. 16b). The drought area in the Maritime Continent also extends westward to 10°S, 80°E over the southern Indian Ocean. Stronger northwestward-propagating ISO is found to the east of the Philippines. La Niña casts an inverse impact on both the mean state and the ISO modes.

The linkage between ENSO and the northwestward-propagating ISO in the WNP can be explained by the vertical wind shear mechanism. The El Niño–induced lower-level westerly and upper-level easterly turn the mean vertical wind shear into easterly shear, which effectively enhances Rossby wave in the lower troposphere. Consequently, stronger ISO is found to migrate northwestward from the equator to the Philippines. The wind shear mechanism also explains why the interannual variations of the ISO in the Indian monsoon region are less pronounced and less sensitive to ENSO compared with that in the WNP.

During El Niño, the enhancement of the MJO in May–July cannot be explained by the vertical shear mechanism because the change in vertical shear does not affect the equatorial Kelvin wave (Wang and Xie 1996). However, El Niño suppresses May–July mean rainfall over Indonesia and enhances mean rainfall in the equatorial western Indian Ocean and the equatorial central-western Pacific (Fig. 16a). On the intraseasonal timescale, the total 10–90-day OLR variances increase between 30° and 90°E and between 140°E and 180°. Due to a stronger MJO, the local 10–90-day OLR variance does not decrease in the Maritime Continent, although the mean convection drops significantly. The active convection in the western Indian Ocean favors initiation of the MJO, and that in the western and central Pacific facilitates MJO's reintensification. These factors may contribute to the enhancement of the MJO. After the northwestward-propagating ISO dominates in the WNP in August–October, the MJO reaches the weakest phase in the year. Deficient rainfall is found west of Sumatra as El Niño develops. A strong southeasterly wind anomaly is produced over the eastern Indian Ocean, inducing upwelling off the coast of Sumatra and cooling the sea surface to suppress the convection. The MJO's eastward-propagation center also expands to 10°N, accompanied by the annual march of the thermal equator. The involvement of the Asian–Pacific summer monsoon in August–October may also add to the collapse of the MJO–ENSO linkage. All these hypotheses remain to be tested by future studies.

On one hand, the enhanced MJO during May–July of an El Niño results from the remote impacts of initial El Niño. On the other hand, it may contribute to further development of El Niño once the enhanced intraseasonal anomalies travel to the western and central Pacific (Kes-

sler and McPhaden 1995). This implies a possible interaction between ENSO and the MJO.

The northward-propagating ISO in the Indian monsoon region is not affected by ENSO. Compared with that in the WNP, the ENSO-induced circulation change is merely a small fraction of the mean monsoon; thus, the ISO in the Indian monsoon region is less sensitive to ENSO effects. The present study provides a useful method to quantify the strength of the northward-propagating ISO. Factors that control the variability of the ISO in the Indian monsoon region remain to be further investigated.

The present wavenumber–frequency spectral analysis allows the quantitative description of intraseasonal wave characteristics, yet it has its own limitation. The method can only distinguish one-dimensional wave propagation, either in the zonal or the meridional direction. In the WNP, when the ISO propagates northwestward, the assessment made from separate analyses of the zonal and meridional components may induce errors concerning the wavenumber and frequency. The results will be substantiated if the analysis method can be extended into two dimensions. The current analysis on the northward-propagating ISO focuses only on the wavenumber-1 anomaly. Whether the method can be applied to investigate higher-wavenumber northward-propagating anomalies at a finite domain needs to be further examined.

The close linkage between the May–July MJO and ENSO sharply contrasts the previous findings that the wintertime MJO is not related to ENSO. This is also confirmed by our November–April MJO index, which generally agrees with the Slingo et al. (1999) index. The different interannual variations of the MJO in November–April, May–July, and August–October suggest that a seasonal stratification of the MJO is necessary in order to investigate its interannual variations. Our explanation of why a developing El Niño can enhance the May–July MJO only advanced a hypothesis. In order to fully understand the mechanism, and explain why the MJO shows different sensitivity to ENSO in different seasons, further numerical and theoretical studies are required.

Acknowledgments. The authors are grateful to Dr. Matthew Wheeler for providing his code of the wavenumber-frequency filter. We thank Dr. H. Hendon for his comments that led to an improved version of the manuscript. This research was supported by the Climate Dynamics Program, National Science Foundation under Grants ATM0073023. The second author is affiliated with International Pacific Research Center (IPRC), which is sponsored in part by the Frontier Research System for Global Change.

REFERENCES

Annamalai, H., and J. M. Slingo, 2001: Active/break cycles: Diagnosis of the intraseasonal variability of the Asian summer monsoon. *Climate Dyn.,* **18,** 85–102.

Anyamba, E. K., and B. C. Weare, 1995: Temporal variability of the 40–50 day oscillation in tropical convection. *Int. J. Climatol.,* **15,** 379–402.

Chen, T.-C., and S.-P. Weng, 1999: Interannual and intraseasonal variations in monsoon depressions and their westward-propagating predecessors. *Mon. Wea. Rev.,* **127,** 1005–1020.

Fink, A., and E. Speth, 1997: Some potential forcing mechanisms of the year-to-year variability of the tropical convection and its intraseasonal (25–70-day) variability. *Int. J. Climatol.,* **17,** 1513–1534.

Frank, W. M., 1987: Tropical cyclone formation. *A Global View of Tropical Cyclones,* R. L. Elsberry et al., Eds., University of Chicago Press, 53–90.

Gutzler, D. S., 1991: Interannual fluctuations of intraseasonal variance of near-equatorial zonal winds. *J. Geophys. Res.,* **96,** 3173–3185.

Hayashi, Y., 1982: Space–time spectral analysis and its applications to atmospheric waves. *J. Meteor. Soc. Japan,* **60,** 156–171.

Hendon, H., C. Zhang, and J. Glick, 1999: Interannual variation of the Madden–Julian Oscillation during austral summer. *J. Climate,* **12,** 2538–2550.

Kalnay, E., and Coauthors, 1996: The NCEP/NCAR 40-Year Reanalysis Project. *Bull. Amer. Meteor. Soc.,* **77,** 437–471.

Kemball-Cook, S., and B. Wang, 2001: Equatorial waves and air–sea interaction in the boreal summer intraseasonal oscillation. *J. Climate,* **14,** 2923–2942.

Kessler, W. S., 2001: EOF representations of the Madden–Julian Oscillation and its connection with ENSO. *J. Climate,* **14,** 3055–3061.

——, and M. J. McPhaden, 1995: Oceanic equatorial waves and the 1991–93 El Niño. *J. Climate,* **8,** 1757–1776.

Krishnamurti, T. N., and P. Ardanuy, 1980: The 10- to 20-day westward propagating mode and ''breaks in the Monsoons.'' *Tellus,* **32,** 15–26.

——, and D. Subrahmanyam, 1982: The 30–50 day mode at 850 mb during MONEX. *J. Atmos. Sci.,* **39,** 2088–2095.

Lau, K.-H., and N.-C. Lau, 1990: Observed structure and propagation characteristics of tropical summertime synoptic scale disturbances. *Mon. Wea. Rev.,* **118,** 1888–1913.

Lau, K.-M., and P. H. Chan, 1986: Aspects of the 40–50 day oscillation during the northern summer as inferred from outgoing longwave radiation. *Mon. Wea. Rev.,* **114,** 1354–1367.

Li, T., and B. Wang, 1994: The influence of sea surface temperature on the tropical intraseasonal oscillation: A numerical study. *Mon. Wea. Rev.,* **122,** 2349–2362.

Liebmann, B., and C. A. Smith, 1996: Description of a complete (interpolated) outgoing longwave radiation dataset. *Bull. Amer. Meteor. Soc.,* **77,** 1275–1277.

LinHo, and B. Wang, 2002: The time–space structure of the Asian–Pacific summer monsoon: A fast annual cycle view. *J. Climate,* **15,** 2001–2019.

Madden, R. A., and P. R. Julian, 1971: Detection of a 40–50 day oscillation in the zonal wind in the tropical Pacific. *J. Atmos. Sci.,* **28,** 702–708.

——, and ——, 1972: Description of global-scale circulation cells in the Tropics with a 40–50 day period. *J. Atmos. Sci.,* **29,** 1109–1123.

Matsuno, T., 1966: Quasi-geostrophic motions in the equatorial area. *J. Meteor. Soc. Japan,* **44,** 25–43.

Mehta, A. V., and T. N. Krishnamurti, 1988: Interannual variability of the 30 to 50 day wave motions. *J. Meteor. Soc. Japan,* **66,** 535–547.

Murakami, T., T. Nakazawa, and J. He, 1984: On the 40–50 day oscillation during the 1979 Northern Hemisphere summer. *J. Meteor. Soc. Japan,* **62,** 440–468.

Nitta, T., 1987: Convective activities in the tropical western Pacific and their impact on the Northern Hemisphere summer circulation. *J. Meteor. Soc. Japan,* **65,** 373–389.

Salby, M. L., and H. H. Hendon, 1994: Intraseasonal behavior of clouds, temperature, and motion in the Tropics. *J. Atmos. Sci.,* **51,** 2207–2224.

Schrage, J., and D. G. Vincent, 1996: Tropical convection on 7–21-day timescales over the western Pacific. *J. Climate*, **9,** 587–607.

Slingo, J. M., D. P. Rowell, K. R. Sperber, and F. Nortley, 1999: On the predictability of the interannual behavior of the Madden–Julian oscillation and its relationship with El Niño. *Quart. J. Roy. Meteor. Soc.,* **125,** 583–609.

Vernekar, A. D., V. Thapliyal, R. H. Kripalani, S. V. Sigh, and B. Kirtman, 1993: Global structure of the Madden–Julian Oscillations during two recent contrasting summer monsoon seasons over India. *Meteor. Atmos. Phys.,* **52,** 37–47.

von Storch, H., and F. W. Zwiers, 1999: *Statistical Analysis for Climate Research.* Cambridge University Press, 484 pp.

Wang, B., and H. Rui, 1990: Synoptic climatology of transient tropical intraseasonal convection anomalies: 1975–1985. *Meteor. Atmos. Phys.,* **44,** 43–61.

——, and X. Xie, 1996: Low-frequency equatorial waves in vertically sheared zonal flow. Part I: Stable waves. *J. Atmos. Sci.,* **53,** 449–467.

——, and ——, 1997: A model for the boreal summer intraseasonal oscillation. *J. Atmos. Sci.,* **54,** 72–86.

——, and Z. Fan, 1999: Choice of South Asian summer monsoon indices. *Bull. Amer. Meteor. Soc.,* **80,** 629–638.

Wheeler, M., and G. N. Kiladis, 1999: Convectively coupled equatorial waves: Analysis of clouds and temperature in the wavenumber–frequency domain. *J. Atmos. Sci.,* **56,** 374–399.

Wilks, D. S., 1995: *Statistical Methods in the Atmospheric Sciences.* Academic Press, 467 pp.

Xie, P., and P. A. Arkin, 1997: Global precipitation: A 17-year monthly analysis based on gauge observations, satellite estimates and numerical model outputs. *Bull. Amer. Meteor. Soc.,* **78,** 2539–2558.

Xie, X., and B. Wang, 1996: Low-frequency equatorial waves in vertically sheared zonal flow. Part II: Unstable waves. *J. Atmos. Sci.,* **53,** 3589–3605.

Yasunari, T., 1979: Cloudiness fluctuations associated with the Northern Hemisphere summer monsoon. *J. Meteor. Soc. Japan,* **57,** 227–242.

——, 1980: A quasi-stationary appearance of 30 to 40 day period in the cloudiness fluctuations during the summer monsoon over India. *J. Meteor. Soc. Japan,* **58,** 225–229.